

Numerical investigation of the steady viscous flow past a stationary deformable bubble

By C. I. CHRISTOV

Department of Fluid Mechanics, Institute of Mechanics and Biomechanics,
Bulgarian Academy of Sciences, P.O. Box 373, Sofia 1090

AND P. K. VOLKOV

Institute of Theoretical and Applied Mechanics, Siberian Branch of the Academy of Sciences
of the USSR, ul. Institutskaya 4/1, Novosibirsk 630090

(Received 22 February 1984 and in revised form 7 January 1985)

A method for solving the Navier–Stokes equations in domains with moving boundaries is proposed. By means of a coordinate transformation, the region under consideration is converted to a region with known boundaries which are coordinate surfaces. An appropriate difference scheme with an algorithm for its implementation is constructed. The method is applied to the case of steady incompressible viscous flow past a resting deformable bubble. Results are obtained for wide ranges for Reynolds and Weber numbers and compared with other theoretical or experimental works in the common regions for the governing parameters. A separation of the flow and the occurrence of a toroidal vortex in the rear of the bubble is observed and verified through a number of computations. Typical flow patterns as well as a variety of practically important relations between the parameters of the flow are shown graphically.

1. Introduction

Recently the steady rise of drops and bubbles in viscous liquids has been intensively studied both theoretically and experimentally, but the knowledge gathered about the shape of bubble and patterns of the flow is still not great. Experimental studies devoted to the motion of deformable drops or bubbles have been chiefly concerned with the estimation of the terminal velocity of rise (fall). Only recently has some quantitative information concerning the shape of bubbles and the streamlines of the flow been experimentally collected (see Bhaga & Weber 1981). Strictly speaking, the experiments are not solely concerned with the steady rise, since during the motion a bubble passes to regions of lower pressure, and hence the bubble volume increases. So the approximation of steady rise of a bubble is valid only when the radius of the bubble is significantly smaller than the characteristic lengthscale of the pressure gradient. Only when this condition holds may one ‘reverse’ the problem and consider steady flow past a resting bubble as a model of the real physical situation.

The number of theoretical papers dealing with ideal flow about bubbles and drops is large at a time when viscous flow past deformable bubbles and drops is more seldom investigated. This is connected with the formidable difficulties that are encountered in solving the Navier–Stokes equations with deformable free boundaries. For this reason a number of limiting cases have been treated theoretically: low or high

Reynolds numbers in various combinations with or without deformability of the bubble surface.

Levich (1959) solved the problem of boundary-layer flow past a spherical non-deformable bubble – very high Reynolds numbers and very low Weber numbers. Moore (1965) acknowledged to some extent the deformation of the bubble surface, considering the boundary layer around an elliptic gas bubble. El Sawi (1974) extended Moore's analysis and accounted for the interaction between the boundary layer and the shape of the bubble.

The other extreme – low Reynolds numbers – was initially treated by Hadamard (1911) and Rybczynski (1911), who independently derived a solution of the Stokes equations for the case of a non-deformable spherical droplet moving steadily through a quiescent viscous liquid. Taylor & Acrivos (1964) calculated the slight changes in drop shape due to the pressure distribution for the case of small Weber numbers. They also took into consideration some inertial effects by solving the Oseen equations. They presumed that $We = O(Re^2)$ and obtained a solution asymptotically valid up to $O(We^2/Re)$. Further, Brabston & Keller (1975) developed a semianalytical method for intermediate Reynolds numbers (up to 80) and negligible Weber numbers (spherical shape).

Summarizing the abovementioned results as well as some other works, it can be concluded that until now in the case of viscous flow the shape of the bubble (droplet) has been considered as unknown only for low Weber numbers. Moreover, this has been done only for the two extreme cases: very low and very high Reynolds numbers. No deformability has been taken into account for intermediate Reynolds numbers. In the present paper a direct numerical method for solving the Navier–Stokes equations in the presence of free deformable boundaries is proposed in order to fill the gap in theoretical results for intermediate Reynolds and Weber numbers. The problem of moving boundaries is tackled by means of an appropriate coordinate transformation.

2. Governing equations and boundary conditions

Let an unbounded volume of viscous incompressible liquid move stationarily with a velocity U_∞ at infinity. Without loss of generality, one can assume that U_∞ is parallel to the coordinate axis Oz . Let there be a resting bubble Ω , which surrounds the origin O of the coordinate system (see figure 1), with its mass centre coinciding with the origin. It is then convenient to employ spherical coordinates:

$$x = r \sin \theta \cos \phi, \quad y = r \sin \theta \sin \phi, \quad z = r \cos \theta$$

with origin at O . The flow is considered to possess axial symmetry with respect to the axis Oz . This means independence from the polar angle ϕ . Assuming also that the flow is not swirling, one can set the circumferential velocity component v_ϕ equal to zero. Then a stream function is introduced according to the formulae

$$v_r = \frac{1}{r^2 \sin \theta} \frac{\partial \psi}{\partial \theta}, \quad v_\theta = -\frac{1}{r \sin \theta} \frac{\partial \psi}{\partial r}, \quad (2.1)$$

and the two-dimensional Navier–Stokes equations are recast in the form

$$\frac{1}{r^2 \sin \theta} \left[\psi_\theta \zeta_r - \psi_r \zeta_\theta - \frac{\zeta}{r} \psi_\theta + \zeta \cot \theta \psi_r \right] = \nu \left[D^2 \zeta + \frac{2}{r} \zeta_r - \frac{\zeta}{r^2 \sin \theta} + \frac{2 \cot \theta}{r^2} \zeta_\theta \right], \quad (2.2)$$

$$D^2 \psi = -2r \sin \theta \zeta, \quad (2.3)$$

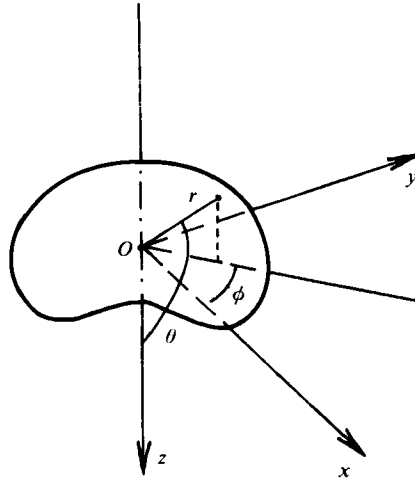


FIGURE 1. Geometry of the flow and coordinate system.

where the Stokesian operator is denoted by

$$D^2 \equiv \frac{\partial^2}{\partial r^2} + \frac{\sin \theta}{r^2} \frac{\partial}{\partial \theta} \left(\frac{1}{\sin \theta} \frac{\partial}{\partial \theta} \right).$$

In the above equations ζ is the vorticity function and subscripts θ and r denote partial differentiation with respect to these variables.

The first boundary condition acknowledges the fact that at infinity liquid moves with a uniform velocity U_∞ in the z -direction:

$$\psi(r, \theta) \rightarrow \frac{1}{2} U_\infty r^2 \sin^2 \theta, \quad \zeta \rightarrow 0 \quad \text{at } r \rightarrow \infty. \quad (2.4a)$$

Numerical implementation of this condition requires that the region be cut at a certain $r = r_\infty$, this being of crucial importance for the efficiency of the calculations. So it is worthwhile to find a way to improve the condition (2.4a) in a manner that allows a good accuracy even in not very large regions. One of the ways of doing this is to consider an Oseen type of flow at large r . As suggested by Burgers (see Happel & Brenner 1965), the flow at infinity can be thought of as created from a point force applied to the origin of the coordinate system. The magnitude of this force is equal to the drag force exerted by the liquid on the bubble (for details see the Appendix). On the other hand, the drag force is equal to the buoyancy force, and therefore

$$\left. \begin{aligned} \psi(r, \theta) &\rightarrow \frac{1}{2} U_\infty r^2 \sin^2 \theta - \frac{gV}{4\pi U_\infty} (1 + \cos \theta) \left\{ 1 - \exp \left[-\frac{rU_\infty}{\nu} (1 - \cos \theta) \right] \right\}, \\ \zeta(r, \theta) &\rightarrow -\frac{gVU_\infty}{4\pi\nu^2} \frac{\sin \theta}{r} \left(1 + \frac{\nu}{rU_\infty} \right) \exp \left[-\frac{rU_\infty}{\nu} (1 - \cos \theta) \right] \quad \text{as } r \rightarrow \infty. \end{aligned} \right\} \quad (2.4b)$$

where g is the acceleration due to gravity and V is the volume of the bubble. The density of the gas inside the bubble is neglected in comparison with the density of fluid.

The other set of boundary conditions refers to the bubble surface Γ (see figure 1). Let the equation of this surface be

$$r = R(\theta). \quad (2.5)$$

This expression holds only for a starlike region. In the present paper we restrict ourselves only to bubbles with starlike shapes.

As the flow is steady, the bubble boundary appears to be a stream surface, i.e. for every value of ϕ the curve Γ is a streamline, so

$$\psi(R(\theta), \theta) = 0, \tag{2.6}$$

which is the first boundary condition on the bubble surface. The second boundary condition reflects the facts that the gas inside the bubble is inviscid and the surface exhibits no intrinsic shear or dilational viscosities. As a result, the tangential components of the stress vector have to be equal to zero at the bubble surface:

$$\zeta + \frac{\psi_r}{R^2(\theta) \sin \theta} \frac{1 + 2R'{}^2(\theta)/R^2(\theta) - R''(\theta)/R(\theta)}{1 + R'{}^2(\theta)/R^2(\theta)} = 0. \tag{2.7}$$

The third boundary condition represents the balance of normal components of the stress vectors of the two phases at the bubble boundary. After trivial manipulations involving (2.7), one obtains from the balance of normal stresses the following:

$$-p(R(\theta), \theta) + 2\mu \left[\frac{\psi_{\theta r} - (\psi_{\theta}/R) + R'\psi_{rr}}{R^2 \sin \theta} + \frac{R'}{R} \zeta \right] = \sigma \kappa - p_b, \tag{2.8}$$

where p_b is the thermodynamic pressure in the bubble, σ is the surface tension and κ is the curvature of the surface:

$$\kappa = \frac{R^2 + 2R'{}^2 - RR''}{(R^2 + R'{}^2)^{3/2}} + \frac{|R' \cos \theta - R \sin \theta|}{R \sin \theta (R^2 + R'{}^2)^{3/2}}.$$

It is convenient to introduce a new dependent variable

$$p = q + r g \rho \cos \theta + p_{\infty}, \quad p_{\infty} = p(r \rightarrow \infty, \theta = \frac{1}{2}\pi), \tag{2.9}$$

in order to simplify the calculations. q is just the deviation due to dynamics from the equilibrium pressure distribution that is generated by the gravity force. The magnitude of the pressure at infinity cannot be disregarded, because of the presence of the bubble. In fact the interaction between the pressure difference $p_b - p_{\infty}$ and the surface tension σ governs the bubble size, and the ratio of these two quantities defines a characteristic lengthscale of the problem. For the sake of comparison with experimental work, however, the diameter of the equivalent spherical bubble (with the same volume) is selected for the reference length. For the radius of the equivalent bubble we have

$$a = \left(\frac{3}{4\pi} V \right)^{1/3}, \tag{2.10}$$

where V is the volume of the bubble and is given by

$$V = \frac{2\pi}{3} \int_0^{\pi} R^3(\theta) \sin \theta \, d\theta. \tag{2.11}$$

Equations are rendered dimensionless by means of the transformation

$$r = 2ar', \quad \psi = (2a)^2 U_{\infty} \psi', \quad \zeta = (2a)^{-1} U_{\infty} \zeta', \quad R = 2aR', \quad q = p U_{\infty}^2 q', \tag{2.12}$$

and primes are henceforth omitted, without fear of confusion. The transformed equations are

$$\frac{Re}{r^2 \sin \theta} \left[\psi_{\theta} \zeta_r - \psi_r \zeta_{\theta} - \frac{\zeta}{r} \psi_{\theta} + \zeta \cot \theta \psi_r \right] = D^2 \zeta + \frac{2}{r} \zeta_r + \frac{2 \cot \theta}{r^2} \zeta_{\theta} - \frac{\zeta}{r^2 \sin \theta}, \tag{2.13}$$

$$D^2\psi = -2r \sin \theta \zeta, \tag{2.14}$$

$$\psi(r, \theta) \rightarrow \frac{1}{2}r^2 \sin^2 \theta, \quad \zeta \rightarrow 0 \quad \text{at } r \rightarrow \infty, \tag{2.15a}$$

$$\left. \begin{aligned} \psi(r, \theta) &\rightarrow \frac{1}{2}r^2 \sin^2 \theta - \frac{1}{Fr} \frac{V}{4\pi} (1 + \cos \theta) \{1 - \exp[-r Re(1 - \cos \theta)]\}, \\ \zeta(r, \theta) &\rightarrow -\frac{\sin \theta}{r} \left(1 + \frac{1}{Re}\right) \frac{Re^2 V}{Fr 4\pi} \exp[-r Re(1 - \cos \theta)], \quad \text{at } r \rightarrow \infty. \end{aligned} \right\} \tag{2.15b}$$

$$\psi(R(\theta), \theta) = 0, \tag{2.16}$$

$$\zeta + \frac{\psi_r}{R^2 \sin \theta} \frac{1 + 2R'^2 R^{-2} - R'' R^{-1}}{1 + R'^2 R^{-2}} = 0 \quad \text{at } r = R(\theta), \tag{2.17}$$

$$\begin{aligned} -q - \frac{R \cos \theta}{Fr} + \frac{2}{Re} \left[\frac{\psi_{\theta r} - \psi_{\theta} R^{-1} + R' \psi_{rr}}{R^2 \sin \theta} + \frac{R'}{R} \zeta \right] \\ = \frac{1}{We} \left[\frac{R^2 + 2R'^2 - RR''}{(R^2 + R'^2)^{\frac{3}{2}}} - \frac{|R' \cos \theta - R \sin \theta|}{R \sin \theta (R^2 + R'^2)^{\frac{1}{2}}} - P_d \right], \end{aligned} \tag{2.18}$$

where

$$Fr = \frac{U_{\infty}^2}{2ga} \quad \text{is the Froude number,}$$

$$Re = \frac{2U_{\infty} a}{\psi} \quad \text{is the Reynolds number,}$$

$$We = \frac{2\rho U_{\infty}^2 a}{\sigma} \quad \text{is the Weber number,}$$

$$P_d = \frac{2a(p_b - p_{\infty})}{\sigma} \quad \text{is the dimensionless pressure difference.}$$

3. Coordinate transformation

Equations (2.13)–(2.18) form a coupled boundary-value problem for estimating the stream function, vorticity function and the shape of the bubble. The latter has to be calculated implicitly from the set of boundary conditions (2.16)–(2.18). This set consists of three equations for the boundary magnitudes of the two unknown bulk quantities ψ and ζ , and the boundary-value problem is correct only if the shape of the bubble $r = R(\theta)$ is an unknown function. The implicit manner of computing of $R(\theta)$ erects a lot of obstacles in the way of numerical solution. In addition, the presence of an unknown boundary that is not a coordinate line complicates the numerical scheme and algorithm considerably. For this reason a transformation of the independent variable is introduced:

$$r = \eta R(\theta), \quad \theta = \theta. \tag{3.1}$$

Although apparently simple, the last transformation has turned out to be very helpful in investigating the correctness of the mathematical problem stated above (see Pukhnatchov 1974). It has also been successfully employed by the authors (see Volkov, Kouznetsov & Christov 1980; Volkov & Christov 1980) in the numerical treatment of the problems of unsteady and steady rise of a bubble through inviscid

liquid. In terms of the new independent variables, the boundary-value problem (2.13)–(2.18) takes the form

$$\begin{aligned} & \left(1 + \frac{R'^2}{R^2}\right) \frac{\partial^2 \zeta}{\partial \eta^2} + \frac{\sin \theta}{\eta^2} \frac{\partial}{\partial \theta} \left(\frac{1}{\sin \theta} \frac{\partial \zeta}{\partial \theta} \right) - 2 \frac{R'}{R\eta} \frac{\partial^2 \zeta}{\partial \eta \partial \theta} \\ & + \frac{1}{\eta} \left(-\frac{R''}{R} + 2 \frac{R'^2}{R^2} + \frac{R'}{R} \cot \theta + 2 \right) \frac{\partial \zeta}{\partial \eta} - \frac{\zeta}{\eta^2 \sin \theta} + 2 \frac{\cot \theta}{\eta} \left(\zeta_\theta - \eta \frac{R'}{R} \zeta_\eta \right) \\ & = \frac{Re}{\eta^2 \sin \theta} \left[\left(\psi_\theta - \eta \frac{R'}{R} \psi_\eta \right) \left(\zeta_\eta - \frac{1}{\eta} \zeta \right) - \psi_\eta \left(\zeta_\theta - \eta \frac{R'}{R} \zeta_\eta \right) + \zeta \psi_\eta \cot \theta \right], \end{aligned} \tag{3.2}$$

$$\begin{aligned} & \left(1 + \frac{R'^2}{R^2}\right) \psi_{\eta\eta} + \frac{\sin \theta}{\eta^2} \frac{\partial}{\partial \theta} \left(\frac{1}{\sin \theta} \frac{\partial \psi}{\partial \theta} \right) - 2 \frac{R'}{R\eta} \frac{\partial^2 \psi}{\partial \eta \partial \theta} \\ & + \frac{1}{\eta} \left(-\frac{R''}{R} + 2 \frac{R'^2}{R^2} + \frac{R'}{R} \cot \theta + 2 \right) \frac{\partial \psi}{\partial \eta} = -2R^3 \eta \sin \theta \zeta, \end{aligned} \tag{3.3}$$

$$\psi(\eta, \theta) \rightarrow \frac{1}{2} R^2 \eta^2 \sin^2 \theta, \quad \zeta \rightarrow 0 \quad \text{at } \eta \rightarrow \infty, \tag{3.4a}$$

$$\left. \begin{aligned} \psi(\eta, \theta) & \rightarrow \frac{1}{2} R^2 \eta^2 \sin^2 \theta - \frac{1}{Fr} \frac{V}{4\pi} (1 + \cos \theta) \{1 - \exp[-\eta Re R(1 + \cos \theta)]\}, \\ \zeta(\eta, \theta) & \rightarrow -\frac{\sin \theta}{\eta R} \left(1 + \frac{1}{Re}\right) \frac{Re^2}{Fr} \frac{V}{4\pi} \exp[-\eta Re R(1 + \cos \theta)], \quad \text{at } \eta \rightarrow \infty. \end{aligned} \right\} \tag{3.4b}$$

$$\psi(\eta, \theta) = 0 \quad \text{at } \eta = 1, \tag{3.5}$$

$$\zeta + \frac{R^2 + 2R'^2 - RR''}{R^2 + R'^2} \frac{\psi_\eta}{R^2 \sin \theta} = 0 \quad \text{at } \eta = 1, \tag{3.6}$$

$$-q - \frac{R \cos \theta}{Fr} + \frac{2}{Re} \left[\frac{\psi_{\theta\eta}}{R^3 \sin \theta} + \frac{R'}{R} \zeta \right] = \frac{1}{We} \left[\frac{R^2 + 2R'^2 - RR''}{(R^2 + R'^2)^{\frac{3}{2}}} + \frac{|R' \cos \theta - R \sin \theta|}{R \sin \theta (R^2 + R'^2)^{\frac{1}{2}}} - P_d \right]. \tag{3.7}$$

The advantages of the above form of the equations and boundary conditions are obvious:

- (i) a fixed computational domain;
- (ii) an explicit equation (3.7) for estimating the shape $R(\theta)$.

The disadvantages are:

- (i) the equations become somewhat more complicated, showing oblique derivatives;
- (ii) there is a restriction to starlike regions.

The first of these disadvantages proved to be of little importance for the numerical scheme proposed. The second one is also not very restrictive, since instabilities of several different kinds can occur and break the bubble far before the bubble rear can get so close to the bubble cap (very high Weber numbers) and that the bubble becomes concave.

4. Method of solution

In the present paper a numerical solution to the boundary-value problem (3.2)–(3.7) is developed. In the numerical procedure infinity is moved to a certain large value $\eta = \eta_\infty$, and the boundary conditions (3.4) are satisfied there. So the region is reduced to

$$0 \leq \theta \leq \pi, \quad 1 \leq \eta \leq \eta_\infty \tag{4.1}$$

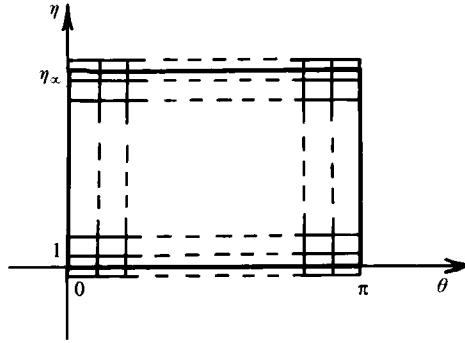


FIGURE 2. Grid in computational domain.

and a uniformly spaced grid is employed (see figure 2):

$$\theta_i = (i-1)h_1, \quad \text{for } i = 1, 2, \dots, M, \tag{4.2a}$$

$$\eta_j = -(j-0.5)h_2 + \eta_\infty, \quad \text{for } j = 1, 2, \dots, N, \tag{4.2b}$$

where $h_1 = \pi/(M-1)$ and $h_2 = (\eta_\infty - 1)/(N-1)$ are the spacings in the θ - and η -directions respectively. The main significance of this mesh is that the boundaries $\eta = 1$ and $\eta = \eta_\infty$ do not coincide with gridlines. Rather they are situated half a step from the nearest gridlines. This proves important in the construction of a second-order approximation to the boundary conditions at the bubble surface.

The solution is divided into three stages. In the first stage (3.2) and (3.3) with boundary conditions (3.4)–(3.6) are solved under the assumption that $R(\theta)$ is a known function. In the second stage the pressure is restored on the basis of the calculated stream function. The calculation of the function $R(\theta)$ from (3.7) when all the other functions are taken as known is the third stage.

4.1. Calculating the values of ψ and ζ

It is readily shown that the continuity of the velocity profile and its symmetry with respect to the axis Oz yield the condition

$$\psi = \zeta = 0 \quad \text{at } \theta = 0, \pi, \tag{4.3}$$

i.e. the boundary-value problem is coupled in the region described in (4.1).

A type of fractional-step method is selected for solution, and hence derivatives with respect to a fictitious time are added to (3.2) and (3.3). The scheme of stabilizing correction is chosen (see Yanenko 1971); this scheme turns out to be stable for reasonable large time steps despite the presence of oblique derivatives.

We now let A_{ij}^α be the magnitude of a certain set function at the stage $t = t_\alpha = (\alpha-1)\tau$, where τ is the time increment. Then the difference scheme of stabilizing correction can be written as

$$\frac{\zeta_{ij}^{l+\frac{1}{2}} - \zeta_{ij}^l}{\tau} = \Lambda_\theta^l \zeta_{ij}^{l+\frac{1}{2}} + \Lambda_\eta \zeta_{ij}^l + F_{ij}^l, \tag{4.4a}$$

$$\frac{\zeta_{ij}^{l+1} - \zeta_{ij}^{l+\frac{1}{2}}}{\tau} = \Lambda_\eta^l (\zeta_{ij}^{l+1} - \zeta_{ij}^l), \tag{4.4b}$$

for $i = 2, \dots, M-1$ and $j = 2, \dots, N-1$.

Boundary conditions for the first half-step are

$$\zeta_{1j}^{l+\frac{1}{2}} = \zeta_{Mj}^{l+\frac{1}{2}} = 0, \quad \text{for } j = 2, \dots, N-1, \tag{4.5a}$$

which come from (4.3). Boundary conditions for the second half-step are

$$\zeta_{ij}^{l+1} = 0, \quad \zeta_{iN}^{l+1} + \zeta_{iN-1}^{l+1} = 2 \left[\frac{3}{2} h_2 f_i^l + (1 - \frac{3}{2} h_2) \frac{\zeta_{iN}^l + \zeta_{iN-1}^l}{2} \right], \tag{4.5b}$$

for $i = 2, \dots, M-1$, where

$$f_i^l = - \left[\frac{1 + 2 \left(\frac{R_{i+1}^l - R_{i-1}^l}{2h_1 R_i^l} \right)^2 - \frac{R_{i+1}^l - 2R_i^l + R_{i-1}^l}{h_1^2 R_i^l}}{1 + \left(\frac{R_{i+1}^l - R_{i-1}^l}{2h_1 R_i^l} \right)^2} \right] \left[\frac{\psi_{iN-1}^l - \psi_{iN}^l}{h_2} \right] / \left[(R_i^l)^2 \sin \theta_i \right].$$

The first of the conditions (4.5b) refers to (3.6), and the second one to (3.4a). Without any difficulties, the condition (3.4b) is implemented when necessary. In (4.4) Λ_θ^l and Λ_η^l are second-order difference approximations to the respective second-order differential operators:

$$\Lambda_\theta^l A = \left\{ \frac{\sin \theta_{i-1}}{\sin \theta_{i-\frac{1}{2}}} A_{i-1/2} - \left[\frac{\sin \theta_{i-1}}{\sin \theta_{i-\frac{1}{2}}} + \frac{\sin \theta_i}{\sin \theta_{i+\frac{1}{2}}} \right] A_{ij} + \frac{\sin \theta_i}{\sin \theta_{i+\frac{1}{2}}} A_{i+1/2} \right\} \frac{1}{\eta_j^2 h_1^2}, \tag{4.6}$$

for $i = 2, \dots, M-1$,

$$\Lambda_\eta^l A = \frac{1}{h_2^2} \left[1 + \left(\frac{R_{i+1}^l - R_{i-1}^l}{2h_1 R_i^l} \right)^2 \right] (A_{ij-1} - 2A_{ij} + A_{ij+1}), \quad \text{for } j = 2, \dots, N-1, \tag{4.7}$$

$$\begin{aligned} F_{ij}^l = & - \frac{R_{i+1}^l - R_{i-1}^l}{h_1 \eta_j R_i^l} \frac{\zeta_{i+1/2}^l - \zeta_{i-1/2}^l}{4h_1 h_2} + \frac{1}{\eta_j} \frac{\zeta_{ij+1}^l - \zeta_{ij-1}^l}{2h_2} \\ & \times \left[- \frac{R_{i+1}^l - 2R_i^l + R_{i-1}^l}{h_1^2 R_i^l} + 2 \left(\frac{R_{i+1}^l - R_{i-1}^l}{2h_1 R_i^l} \right)^2 + 2 + \cot \theta_i \frac{R_{i+1}^l - R_{i-1}^l}{2h_1 R_i^l} \right] \\ & - \frac{\zeta_{ij}^l}{\eta_j^2 \sin \theta_i} + \frac{2 \cot \theta_i}{\eta_j^2} \left(\frac{\zeta_{i+1/2}^l - \zeta_{i-1/2}^l}{2h_1} - \eta_j \frac{R_{i+1}^l - R_{i-1}^l}{2h_1 R_i^l} \frac{\zeta_{ij+1}^l - \zeta_{ij-1}^l}{2h_2} \right) \\ & - \frac{Re}{\eta_j^2 \sin \theta_i} \left[\left(\frac{\psi_{i+1/2}^l - \psi_{i-1/2}^l}{2h_1} - \eta_j \frac{R_{i+1}^l - R_{i-1}^l}{2h_1 R_i^l} \frac{\psi_{ij+1}^l - \psi_{ij-1}^l}{2h_2} \right) \left(\frac{\zeta_{ij+1}^l - \zeta_{ij-1}^l}{2h_2} - \frac{\zeta_{ij}^l}{\eta_j} \right) \right. \\ & \left. - \frac{\psi_{ij+1}^l - \psi_{ij-1}^l}{\eta_j} \left(\frac{\zeta_{i+1/2}^l - \zeta_{i-1/2}^l}{2h_1} - \eta_j \frac{R_{i+1}^l - R_{i-1}^l}{2h_1} \frac{\zeta_{ij+1}^l - \zeta_{ij-1}^l}{2h_2} \right) + \zeta_{ij}^l \cot \theta_i \frac{\psi_{ij+1}^l - \psi_{ij-1}^l}{2h_2} \right]. \end{aligned} \tag{4.8}$$

The approximation to (3.3) is constructed in the same manner:

$$\frac{\psi_{ij}^{l+\frac{1}{2}} - \psi_{ij}^l}{\tau} = \Lambda_\theta^l \psi_{ij}^{l+\frac{1}{2}} + \Lambda_\eta^l \psi_{ij}^l + G_{ij}^l, \tag{4.9a}$$

$$\frac{\psi_{ij}^{l+1} - \psi_{ij}^{l+\frac{1}{2}}}{\tau} = \Lambda_\eta^l (\psi_{ij}^{l+1} - \psi_{ij}^l), \tag{4.9b}$$

for $i = 2, \dots, M-1$ and $j = 2, \dots, N-1$, coupled with the respective boundary conditions

$$\psi_{1j}^{l+\frac{1}{2}} = \psi_{Mj}^{l+\frac{1}{2}} = 0, \quad \text{for } j = 2, \dots, N-1, \tag{4.10a}$$

$$\left. \begin{aligned} & \psi_{iN}^{l+1} + \psi_{iN-1}^{l+1} = 0, \\ & \psi_{i1}^{l+1} = \frac{1}{2} (R_i^l)^2 (\eta_\infty - \frac{1}{2} h_1)^2 \sin^2 \theta_i, \end{aligned} \right\} \text{for } i = 2, \dots, M-1. \tag{4.10b}$$

and

The second equality of (4.10*b*) is an approximation to (3.4*a*). When necessary, (3.4*b*) can be implemented. The scheme (4.9) is coupled by

$$G_{ij}^l = -2 \frac{R_{i+1}^l - R_{i-1}^l}{2h_1 R_i^l \eta_j} \frac{\psi_{i+1j+1}^l - \psi_{i-1j+1}^l - \psi_{i+1j-1}^l + \psi_{i-1j-1}^l}{4h_1 h_2} + \frac{1}{\eta_j} \frac{\psi_{ij+1}^l - \psi_{ij-1}^l}{2h_2} \\ \times \left[-\frac{R_{i+1}^l - 2R_i^l + R_{i-1}^l}{h_1^2} + 2 \left(\frac{R_{i+1}^l - R_{i-1}^l}{2h_1 R_i^l} \right)^2 + \cot \theta_i \frac{R_{i+1}^l - R_{i-1}^l}{2h_1 R_i^l} \right] + 2(R_i^l)^3 \eta_j \sin \theta_i \zeta_{ij}^l. \tag{4.11}$$

4.2. Restoring the pressure

Before turning to (3.7), one needs an explicit expression for the pressure. Such an expression can be derived from the Navier–Stokes equation for the original variables (velocities and pressure) in spherical coordinates. Recalling (3.1), the following equation for the dimensionless function q is derived:

$$\frac{\partial q}{\partial \theta} \Big|_{\eta=1} = -\frac{\partial}{\partial \theta} \frac{v_s^2}{2} + \frac{2}{Re} \left[\left(1 - \frac{R'}{R} \right) \zeta + \left(1 + \frac{R'^2}{R^2} \right) \frac{\partial \zeta}{\partial \eta} - \frac{R'}{R} \frac{\partial \zeta}{\partial \theta} \right]_{\eta=1}, \tag{4.13}$$

where
$$v_s^2 = \frac{1}{R^4 \sin \theta} \left(1 + \frac{R'^2}{R^2} \right) \left(\frac{\partial \psi}{\partial \eta} \right)_{\eta=1}^2,$$

which is an ordinary differential equation. The boundary condition is

$$q = 0 \quad \text{at } \theta = \frac{1}{2}\pi. \tag{4.14}$$

The latter is a straight corollary from the definition (2.9) of q . It is important to note here that the symmetry conditions for q are automatically satisfied because of the structure of (4.13) at $\theta = 0, \pi$.

4.3. Calculating the bubble shape

In this subsection the functions ψ^{l+1} , ζ^{l+1} and q^{l+1} are considered as already known, and a computational procedure for solving (3.7) is outlined. Equation (3.7) is of second order and contains the first and second derivatives of the function $R(\theta)$. In addition it is strongly nonlinear, i.e. an iterative procedure is required for solution. Once again we introduce a fictitious time, starting from the initial condition

$$R^{l,1} = R^l, \tag{4.15}$$

and solve the difference approximation

$$\frac{R_i^{l,k+1} - R_i^{l,k}}{\tau_1} = \frac{R_{i+1}^{l,k+1} - 2R_i^{l,k+1} + R_{i-1}^{l,k+1}}{h_2^2} + c_i \frac{R_{i+1}^{l,k+1} - R_{i-1}^{l,k+1}}{2h_2} - R_i^{l,k+1} + b_i = 0, \\ \text{for } i = 2, 3, \dots, M-1, \tag{4.16}$$

where

$$c_i = 2d_i + 2 \frac{We}{Re} R_i^{l,k} (1 + d_i^2) \frac{\zeta_{iN}^{l+1} + \zeta_{iN-1}^{l+1}}{2}, \\ b_i = (R_i^{l,k})^3 (1 + d_i^2)^{\frac{3}{2}} \left\{ 2 \frac{We}{Re} \frac{\psi_{i+1N-1}^{l+1} - \psi_{i+1N}^{l+1} - \psi_{i-1N-1}^{l+1} + \psi_{i-1N}^{l+1}}{4h_1 h_2 (R_i^{l,k})^3} \right. \\ \left. - \frac{|d_i \cos \theta_i - \sin \theta_i|}{(R_i^{l,k}) (1 + d_i^2)^{\frac{1}{2}} \sin \theta_i} + P_d^{l,k} - We q^{l+1} + We \frac{R^{l,k} \cos \theta_i}{F_{\tau^{l,k}}} \right\}, \\ d_i = \frac{R_{i+1}^{l,k} - R_{i-1}^{l,k}}{2h_2 R_i^{l,k}}.$$

In constructing the difference approximation (4.16), the underlying aim is to obtain as implicit as possible a scheme in order to decrease the constraints on the increment τ_1 of the fictitious time (note that it is different in general from the time step used in solving the Navier–Stokes equations).

As the function $R(\theta)$ has to be smooth at the axis of symmetry of the spherical coordinates, the boundary conditions for $R(\theta)$ are

$$\frac{dR}{d\theta} = 0 \quad \text{at } \theta = 0, \pi,$$

which are approximated as follows:

$$-3R_1 + 4R_2 - R_3 = 0, \quad -3R_M + 4R_{M-1} - R_{M-2} = 0, \quad (4.17)$$

so that (4.16) and (4.17) comprise a coupled linear algebraic system for estimating the values $R_i^{l,k+1}$. It should be mentioned here that for the solution of (4.16) and (4.17) one needs the quantities $F_r^{l,k}$ and $P_d^{l,k}$, which are the current iterations of F_r and P_d . These two are not independent parameters. Rather they are functionals of the flow defined implicitly from two additional constraints imposed on the solution for $R(\theta)$: the first is the requirement that the mass centre of the bubble is situated at the origin of the coordinate system. Formally it is written in the form

$$S_1(F_r, P_d) = \int_0^\pi R^4(\theta) \sin \theta \cos \theta \, d\theta = 0. \quad (4.18)$$

Fulfilment of (4.18) secures the steady character of the computed flow characteristics. In some sense it reflects the fact that the flow velocity U_∞ at infinity (the rising velocity) cannot be an arbitrary value, but depends on Re and We .

The second constraint is the preservation of dimensionless bubble volume, namely

$$S_2(F_r, P_d) = \frac{2\pi}{3} \int_0^\pi R^3(\theta) \sin \theta \, d\theta - 1 = 0. \quad (4.19)$$

This requirement arises from the choice of the characteristic lengthscale of the problem, which is taken to be equal to the radius a of the equivalent spherical bubble. Similarly to the rising velocity U_∞ , the radius a is a functional of the flow, and therefore a function of Re , We and P_d . So one has to vary P_d , unless (4.19) is satisfied, in order to keep the bubble volume constant for different Reynolds and Weber numbers. It should be noted here that (4.19) can be replaced by the equation of state for the gas in the bubble, if necessary.

The adequate incorporation of the constraints (4.18) and (4.19) into the difference scheme for $R(\theta)$ is of crucial importance. An explicit expression for P_d can be derived through multiplying (3.7) by $R^3(\theta) \sin \theta$ and integrating over $\theta \in [0, \pi]$ and taking account of (4.18) and (4.19). Then one gets

$$P_d = \frac{2\pi}{3} We \int_0^\pi R^3(\theta) q|_{\eta=1} \sin \theta \, d\theta - \frac{4\pi}{3} \frac{We}{Re} \int_0^\pi [\psi_{\theta\eta} + R' R^2 \sin \theta \xi]_{\eta=1} \, d\theta \\ + \frac{2\pi}{3} \int_0^\pi \left[\frac{R^2 + 2R'^2 - RR''}{(1 + R'^2/R^2)^{\frac{3}{2}}} \sin \theta + R \frac{|R' \cos \theta - R \sin \theta|}{(1 + R'^2/R^2)^{\frac{1}{2}}} \right] d\theta. \quad (4.20)$$

A difference approximation to (4.20) is readily derived, and will not be discussed here. The important thing here to note is that the value $P_d^{l,k+1}$ is calculated from (4.20), where R is specified as $R^{l,k+1}$. So the only quantity that has not yet been calculated is $F_r^{l,k+1}$. Let us now think of S_1 from (4.18) as a function only of F_r , since P_d is

implicitly related to Fr through (4.20). Then we arrive at the problem of solving the equation

$$S(Fr) \equiv S_1(Fr, P_d(Fr)) = 0$$

simultaneously with (4.16) and (4.17). Once again a fictitious time is introduced:

$$\frac{dS}{dt_1} = -S|S|. \tag{4.21}$$

Obviously, after convergence with respect to time, (4.21) yields (4.18). Moreover, (4.21) is always stable, and its solution tends to zero with $t_1 \rightarrow \infty$ regardless of the initial conditions. On recalling the fact that S is a function of Fr , one obtains

$$\frac{dFr}{dt_1} = -\frac{S|S|}{dS/dFr}, \tag{4.22}$$

which is an explicit relation for estimating Fr . The difference scheme for (4.22) is

$$\frac{Fr^{l,k+1} - Fr^{l,k}}{\tau_1} = -S(Fr^{l,k}) \frac{Fr^{l,k} - Fr^{l,k-1}}{S(Fr^{l,k}) - S(Fr^{l,k-1})} |S(Fr^{l,k})|. \tag{4.23}$$

Since the set function $R^{l,k+1}$ calculated from (4.16) and (4.17) is a function of $Fr^{l,k}$, $S(Fr^{l,k})$ is specified as

$$S(Fr^{l,k}) \equiv \int_0^\pi [R^{l,k+1}(\theta)]^4 \sin \theta \cos \theta \, d\theta.$$

Thus, after $R^{l,k+1}$ has been calculated, $S(Fr^{l,k})$ can also be calculated, and $Fr^{l,k+1}$ can be obtained from (4.23). Thus a full stage of the iteration procedure for estimating $R(\theta)$ is completed.

Iterations are carried out starting from the initial condition (4.15) and the initial conditions for Fr ,

$$Fr^{l,1} = Fr^{l-1,K+1}, \quad Fr^{l,0} = Fr^{l-1,K}, \tag{4.24}$$

until the following criterion is satisfied:

$$\max_i \left| \frac{R_i^{l,k+1} - R_i^{l,k}}{R_i^{l,k+1}} \right| \leq \epsilon \approx 0.0001. \tag{4.25}$$

After that, the following values are assigned:

$$R^{l+1} \equiv R^{l,K+1}, \quad Fr^{l+1} \equiv Fr^{l,K+1}, \quad P_d^{l+1} \equiv P_d^{l,K+1}, \tag{4.26}$$

where K is the first value of k for which (4.25) is satisfied.

So far §§4.1–4.3 have described a full step with respect to the global iteration. Such steps are repeated (increasing the superscript l) until convergence is attained under the provisions of a criterion similar to (4.25). It appears to take about 10–20 global iterations for convergence, with a tendency for a sharp drop of the number of inner iterations after the 3rd–5th global iteration.

5. Tests and comparisons

In order to check the accuracy of the proposed scheme, two different meshes are employed in calculations. The basic mesh (henceforth termed the ‘fine’ mesh) has $M = 29$, $N = 41$. The auxiliary mesh (termed the ‘rougher’ mesh) has $M = 15$, $N = 21$. The spacings of the rougher mesh are selected to be exactly twice as large as those of the fine one. This proves to be convenient when comparing the results.

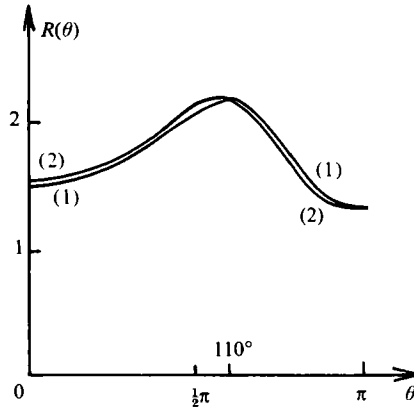


FIGURE 3. Comparison for the bubble shape $R(\theta)$ on two different meshes: (1) 29×41 ; (2) 15×21 . $Re = 8$, $We = 7.2$.

It is interesting to note that changing the mesh size influences most of all the calculation of pressure and bubble shape. The most significant differences between the solutions on the two meshes occur as a rule at the bubble cap $\theta = \pi$. As should be expected, these differences are more conspicuous for higher Weber numbers. Figure 3 shows the shape function $R(\theta)$ obtained on the two different meshes. The Weber number is very high, $We = 7.2$, and the Reynolds number is moderate, $Re = 8$. The difference between the two numerical solutions is less than 3% for the stream function and less than 5.4% for the pressure. The calculated values of the Froude number differ by less than 1%, and those of the pressure-difference parameter P_d by less than 5%. Acknowledging that the rougher mesh is indeed very rough, the comparison of results on the two meshes is quantitatively fully satisfactory and can be viewed as evidence of the good performance of the proposed scheme. It is still important, however, to have the results checked also in some simpler physical situations.

The part of the difference scheme that deals with the calculation of ψ and ζ is checked through solving the problem of steady flow past a resting spherical bubble. In order to solve this problem by means of our algorithm, the shape function $R(\theta)$ is set equal to a constant, instead of calculating it from (3.7). For each of the boundary conditions (3.4*a, b*) the full system of Navier–Stokes equations is solved by means of the difference scheme proposed here, and the drag coefficient is calculated according to the formula

$$C_D = \frac{4g \cdot 2a}{3U_\infty^2} = \frac{4}{3} \frac{1}{Fr}. \quad (5.1)$$

Table 1 shows the computed drag coefficient for a variety of Reynolds numbers and compares them with numerical and asymptotic results of other authors. Our results are obtained with $\eta_\infty = 5$. It is important to note that increasing η_∞ up to 10 improves only the third digit of the drag coefficient, i.e. $\eta_\infty = 5$ is the optimal value. This is not the case, however, when the surface is deformable. The significance of η_∞ in that case will be discussed below.

The part of the difference scheme that is responsible for calculating the bubble shape is tested separately too. For this purpose the gravity is ‘switched off’, taking $Fr^{-1} = 0$ instead of calculating the Froude number from the appropriate equation. Then the drag force is no longer balanced, and the bubble is dragged away from the

<i>Re</i>	Asymptotic solutions		Numerical solution of Brabston & Keller (1975); boundary condition	Present computations; boundary conditions	
	<i>Re</i> ≪ 1 <i>C_D</i> = 8/ <i>Re</i>	<i>Re</i> ≫ 1 Moore (1963)	(3.4 <i>b</i>)	(3.4 <i>b</i>)	(3.4 <i>a</i>)
0.1	80	—	80.83	80.231	102.064
0.5	16	—	16.85	16.483	20.257
1	8	—	8.795	8.439	10.167
5	1.6	—	2.184	1.996	2.491
10	—	0.7222	1.175	1.172	1.279
20	—	0.6068	0.681	0.675	0.780
40	—	0.3903	0.4156	0.398	0.525
60	—	0.2858	0.3001	0.332	0.412
100	—	0.1872	0.1931	0.243	0.259

TABLE 1. Comparison of the drag coefficient

liquid. The bubble shape should remain spherical during such 'frozen' motion. Then, imposing the appropriate initial condition for the global iteration and interpreting the latter as physical time, one arrives at a solution that corresponds to the undisturbed translatory motion of a spherical bubble with velocity equal to the fluid velocity at infinity. This is quite a trivial situation to be treated numerically if only the origin of the coordinate system moves with the mass centre of the bubble. This is not the case, however, when the centre of coordinate system is fixed while the bubble moves. Then the shape function becomes more complicated, deviating considerably from a constant, although the shape itself remains spherical. The situation described is treated by means of the proposed scheme, and calculations are conducted almost up to the moment at which the origin of the coordinate system touches the bubble surface. The shape obtained during this kind of motion turns out to be spherical to within an accuracy of 1%.

So far all major parts of the numerical scheme are tested and verified. Results assure one that the method and scheme proposed are reliable.

6. Results

It is well known that in the limiting case when $Re \rightarrow 0$ the portion of the normal stress that is due to viscous terms is in equilibrium with that due to pressure if the shape of surface is spherical (see Taylor & Acrivos 1964). This means that for each Weber number the spherical surface of a bubble is in equilibrium. The problem is that this equilibrium is stable only for sufficiently low Weber numbers. For higher We a bifurcation of the shape can take place even for very small Reynolds numbers. Moreover, for $Re \rightarrow 0$ (2.18) becomes ill-posed as an equation for estimating the function $R(\theta)$ unless $We = O(Re)$. The present computations confirm this conclusion, and more specifically they support the result of Taylor & Acrivos (1964) that the shape remains spherical when $We = O(Re^2)$. More rigorously, it can be stated that the spherical shape is preserved if the capillary number Ca is small:

$$Ca = \frac{We}{Re} \equiv \frac{\mu U_\infty}{\sigma} \ll 1. \quad (6.1)$$

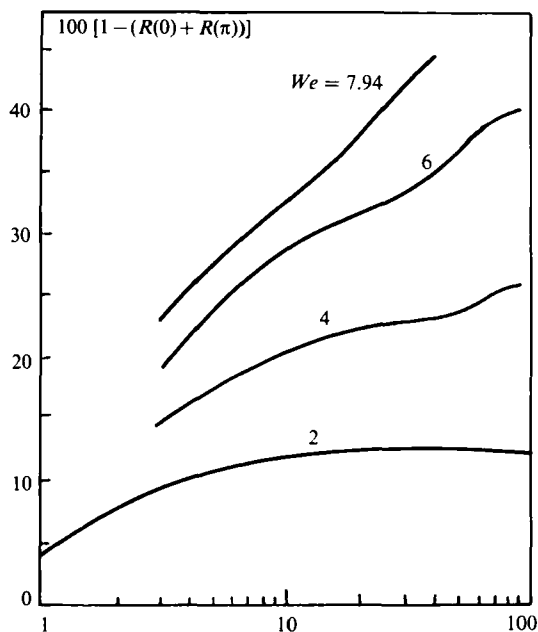


FIGURE 4. Percentage deviation of the vertical diameter of the bubble from that of the equivalent sphere as a function of Re : (1) $We = 2$; (2) 4; (3) 6; (4) 7.94.

For most real liquids the capillary number for which steady rise of bubbles is possible is $Ca \ll 1$, and values of Ca of order unity are very hard to obtain experimentally. Only Bhaga & Weber (1981), making use of polymer solutions, succeeded in increasing μ and decreasing σ enough to be able to investigate experimentally the extremely interesting case $Ca = O(1)$, $We = O(1)$, where the most complex deformation of the bubble shape occurs. Theoretically, the case $Ca = O(1)$ is also a hard problem, and so the known theoretical approaches are concerned with small capillary numbers. These are either investigations concerned with almost ideal flow with $Re \gg 1$ and $Ca \ll 1$, leading to an elliptic shape of bubble, or with Stokes flow with $Re \ll 1$ and $Ca \ll 1$, where the deviation from spherical shape is negligible. Both these cases are satisfactorily treated analytically, but the methods employed are unable to give results for $Ca = O(1)$. That is why it seems important to develop a numerical method for predicting the patterns of the flow and shape in order to fill the gap around $Ca = O(1)$, $We = O(1)$. We therefore focus our attention on this case. In this connection it is important to note that our scheme turns out to be convergent only for $Ca \leq 2.62$, the latter value being attained for $Re = 3$. For the rest of the Reynolds numbers investigated, the maximal value of capillary number that can be reached is approximately $Ca \approx 2.5$. For higher Ca the algorithm ceases to converge, which is not surprising bearing in mind what has been said above about (2.18).

The method proposed here is subject to one more limitation connected with high Reynolds numbers. As always, the calculations with high Reynolds numbers require a very fine mesh, which brings into view the problem of computational time. On the adopted 29×41 mesh we believe that results obtained can be trusted only when $Re \leq 100$ for small Weber numbers, and even only when $Re \leq 40$ for higher Weber numbers. The situation is worsened by the presence of the numerical 'infinity' η_∞ . At high Weber numbers the bubble becomes more oblate, i.e. the shape function $R(\theta)$ becomes significantly less than the equivalent-sphere radius, which puts the 'actual

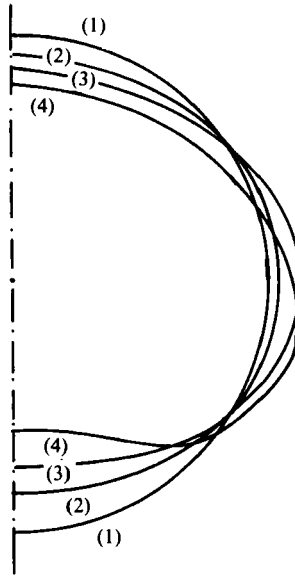


FIGURE 5. Evolution of the bubble shape with Weber number for an intermediate Reynolds number $Re = 12$: (1) $We = 0.04$; (2) 2; (3) 3.2; (4) 7.2.

infinity' at $\eta_\infty R(0)$ in the rear of the bubble. The later value can be as small as $\frac{1}{2}\eta_\infty R(\frac{1}{2}\pi)$, for example. This means that the boundary condition at infinity, namely (3.4), is imposed inappropriately close to the rear end of the bubble. The latter is especially disturbing for high Reynolds numbers, where a separation at the bubble rear occurs. For this reason we varied η_∞ , and it turned out that for $Re = 100$ the optimal value for η_∞ was 18 (compare with the value $\eta_\infty = 5$ in the case of spherical surface). On figure 4 are presented data regarding the maximal deformation (percentage deviation of the vertical diameter of the bubble from that of the equivalent sphere) as a function of Re for a couple of Weber numbers. It is clearly seen that the monotonic behaviour of the curves is disrupted at high Weber and Reynolds numbers. We regard this as a sign of negative effects of the scheme, which take place because of the reasons listed above.

Figure 5 shows the bubble shape for an intermediate Reynolds number $Re = 12$ and different Weber numbers. It is clearly seen that for high Weber numbers the surface even exhibits negative curvature despite still being completely steady and stable. This means that the flow is rearranged in such a way that the viscous portion of the normal stress dominates the pressure portion at the bubble rear and pulls the surface in that region, thus balancing the capillary force.

Figure 6 shows the bubble shape for an intermediate Morton number

$$\mathcal{M} = \frac{We^3}{Re^4 Fr} \equiv \frac{g\mu^4}{\rho\sigma^3}, \quad (6.2)$$

and a couple of Reynolds numbers. As the Morton number specifies the physical properties of a liquid, the presented results concern in fact the development of the bubble shape with bubble size (and hence with terminal rising velocity) for a given liquid.

It is interesting to track the influence of deformation on flow patterns for large Re and We . Figure 7(a-d) show the calculated streamlines for four different Reynolds

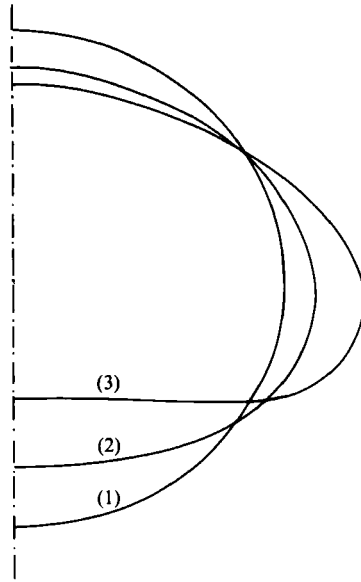


FIGURE 6. Evolution of the bubble shape with Reynolds number for an intermediate Morton number $\mathcal{M} = 0.01$: (1) $Re = 4$, $We = 0.94$; (2) 12, 4.84; (3) 20.87, 9.43.

numbers and sufficiently large Weber number. For convenience when making comparisons with experiments, the respective values of the Morton number are also plotted. It is seen that a toroidal vortex appears at the rear of the bubble. The size of the vortex increases with increasing Reynolds number. Quite similar is the evolution of the toroidal vortex with Weber number for $Re = 60$, displayed on figure 8(a-c). Table 2 shows, as a function of Reynolds number, the smallest value of Weber number for which a toroidal vortex occurs at the rear of the bubble.

In order to shed some more light on the separation phenomena the circumferential velocity component v_θ is plotted on figure 9 for $Re = 12$ and $We = 7.2$. As expected, v_θ changes sign in the separated zone.

The study of separation is completed by the data concerning the angle of separation θ^* , which are plotted on figure 10 and compared with experiments of Bhaga & Weber (1981). Agreement is fair except for $Re \leq 40$. This is natural, since the definition of angle of separation in Bhaga & Weber differs from ours. In the present paper the origin from which the angle is measured is the mass centre of the bubble, while in Bhaga & Weber the origin is the centre of a certain imaginary ellipsoid which comprises the entire bubble and approximates the shape well in the vicinity of the bubble cap. For this reason they can have an angle of separation that is less than 90° , while for our quantity this is the limiting value, which can never be reached.

Another quantity that is often measured in experiments is the so-called aspect ratio h/w , where h is the height of the bubble and w its width. The very name implies that the aspect ratio is applicable only to elliptic or almost-elliptic bubbles. In the present work the bubbles are of general shape, but it is still interesting to compare our results with experimental ones. Figure 11 presents this comparison. Taking into account that experimental values for h and w are in fact the small and large axes of a certain 'equivalent elliptic bubble' the agreement can be pronounced to be good.

In our opinion, a more appropriate characteristic than the aspect ratio is

$$\chi \equiv R(\frac{1}{2}\pi)/R(\pi), \quad (6.3)$$

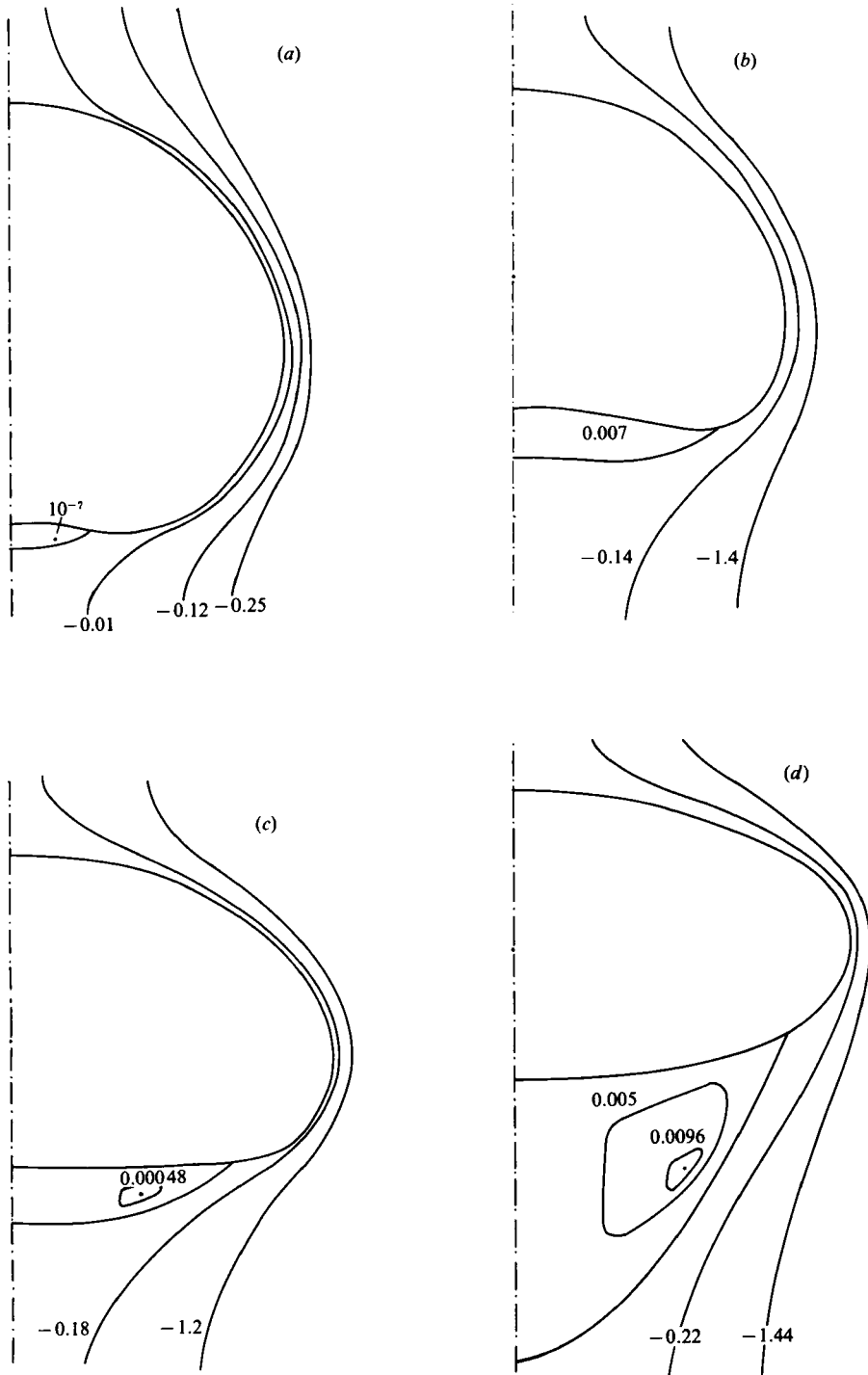


FIGURE 7. Flow patterns for a high Weber number $We = 7.64$: (a) $Re = 3$, $\mathcal{M} = 33$; (b) 9.76 , 0.1 ; (c) 20 , 6.83×10^{-3} ; (d) 40 , 2.69×10^{-4} .

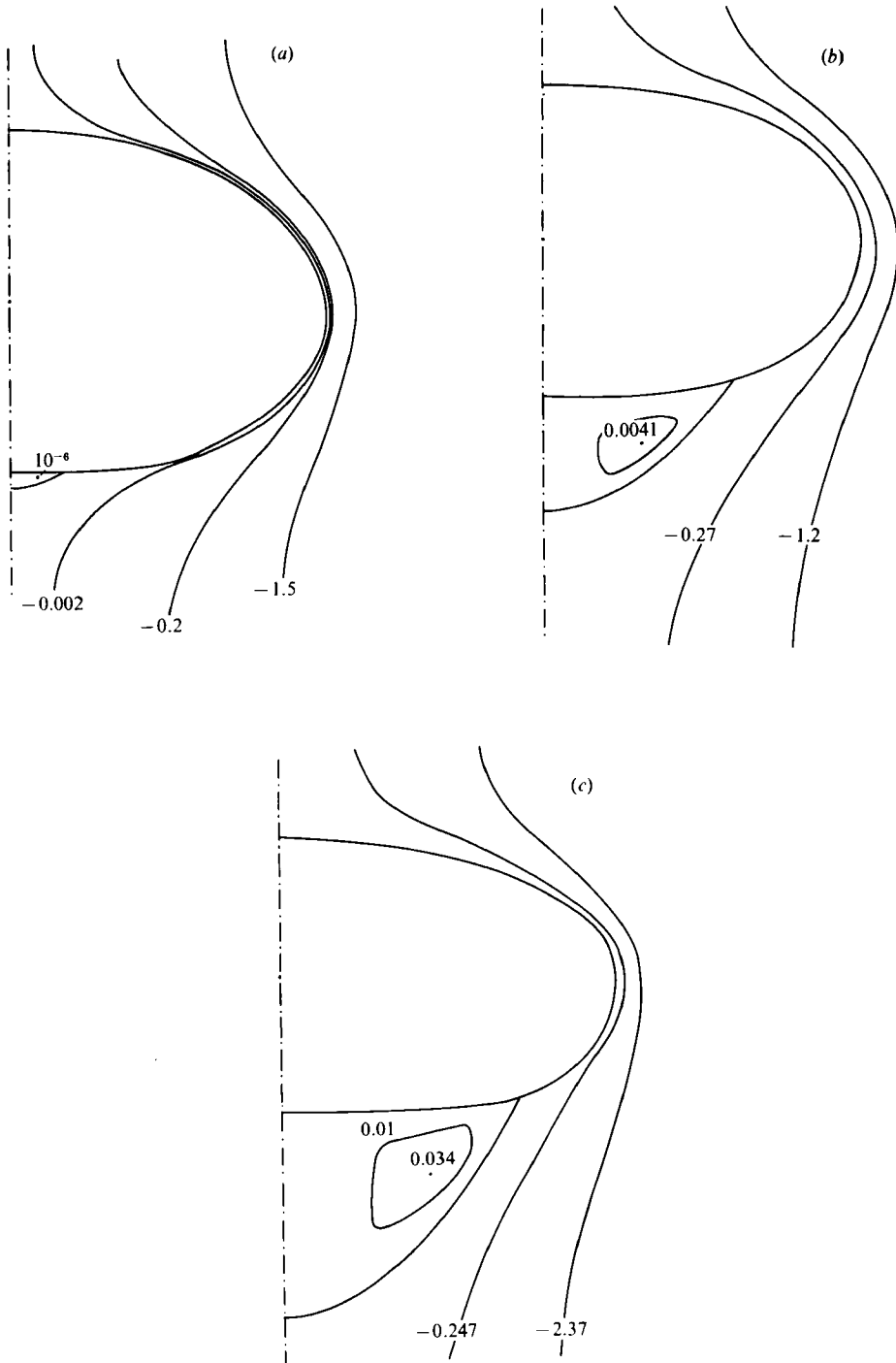
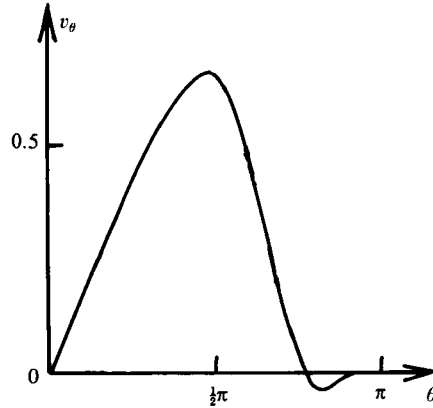
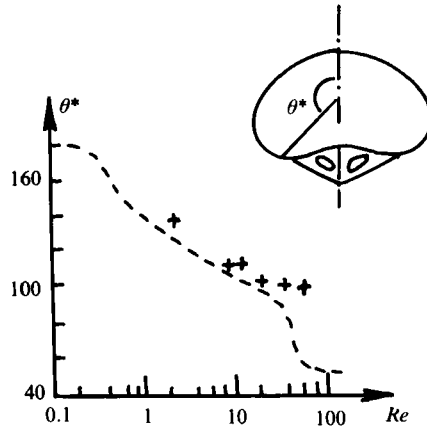


FIGURE 8. Flow patterns for a high Reynolds number $Re = 60$: (a) $We = 5.04$, $\mathcal{M} = 9.3 \times 10^{-6}$; (b) 5.8 , 1.66×10^{-5} ; (c) 6.9 , 3.46×10^{-5} .

Re	3	8	12	20	40	60	100
We_{\min}	8.08	7.66	7.66	7.62	6.54	5.24	5.04

TABLE 2. Minimal Weber number at which the toroidal vortex initially appears

FIGURE 9. Circumferential velocity component v_θ at bubble surface as a function of the angle θ . $Re = 12$, $We = 7.2$.FIGURE 10. Angle of separation θ^* for high Weber number as a function of Reynolds number. $We = 7.68$. Plusses represent the present computations. Dashed line gives the averaged experimental data of Bhaga & Weber (1981) for the value of separation angle measured from the centre of a certain equivalent ellipsoid.

which is well-defined numerically on the one hand, and on the other hand is equal to the aspect ratio in the case of elliptic bubbles. Figure 12 shows χ as a function of Weber number for several different Reynolds numbers. The curve referring to $Re = \infty$ is the result for the ideal flow computed by Volkov & Christov (1980). It is clearly seen that the curvatures of curves presented on figure 12 change sign to that which is characteristic of the ideal flow after $Re > 12$, but the respective ordinates are still well separated from those for the ideal flow, even for $Re = 100$. This means that the practical limit for which the viscous flow approaches the ideal one lies well beyond $Re = 100$. The reason for this might well be that the theoretically investigated

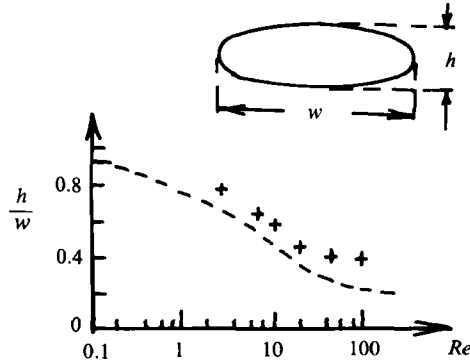


FIGURE 11. Aspect ratio for high Weber number $We = 7.64$ as a function of Reynolds number. Plusses represent the present computations. Dashed line gives the averaged experimental data of Bhaga & Weber (1981).

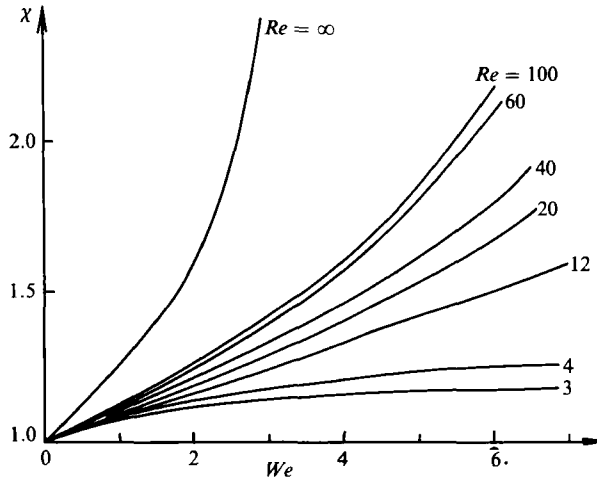


FIGURE 12. The ratio χ as a function of Weber number for different Reynolds numbers. The curve $Re = \infty$ is from the ideal-flow computations of Volkov & Christov (1980).

ideal flows are without separation, while the limiting case for the viscous flows considered here could be a separated ideal flow. This speculation, however, does not explain the closeness of curves for $Re = 60$ and $Re = 100$. We attribute this to scheme limitations, namely to the scheme viscosity, which becomes important for $Re \geq 60$ and results in a decrease of the actual value of the Reynolds number.

The same tendency is observed on figure 13, which shows χ as a function of We for different Morton numbers. Curves 1 and 2 present our computations, while 3–5 are from the paper of Miksis, Vanden-Broeck & Keller (1982). The discrepancy between the two results is due to the fact that the solution of Miksis *et al.* is based on perturbing the ideal-flow bubble shape, and so it is natural that their results are much closer to the ideal-flow curve 5 ($\mathcal{M} = 0$).

Finally, it is interesting to note that the present algorithm is capable of predicting the terminal rise velocity. The latter is the main objective of a number of experimental works (see Bhaga & Weber 1981; Belov, Elovikov & Okulov 1975; Gorodetzskaya 1949; Haberman & Morton 1954; Jezdinsky & Rudis 1973; Kutateladze & Nakoryakov 1984). In different experimental works various regimes of a number of different

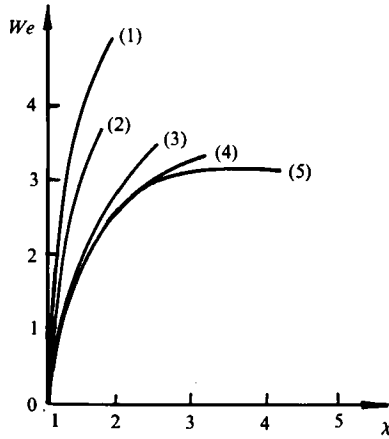


FIGURE 13. Calculated ratio χ (curves 1 and 2) for different Morton numbers compared with results of Miksis *et al.* (1982) (curves 3–5): (1) $\mathcal{M} = 10^{-5}$; (2) 1.8×10^{-7} ; (3) 10^{-5} ; (4) 1.75×10^{-7} ; (5) 0.

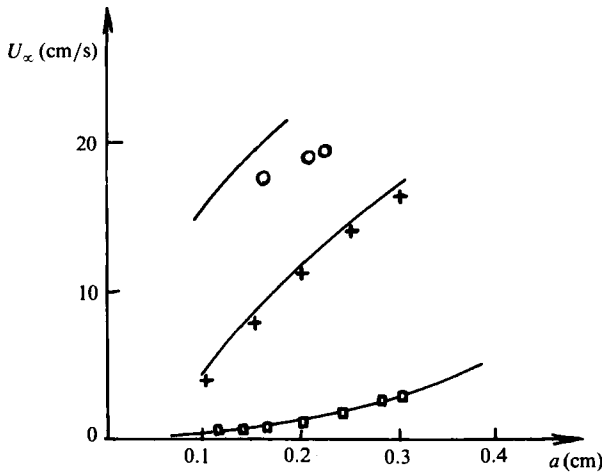


FIGURE 14. Rise velocity U_∞ as a function of the radius of the equivalent sphere: \circ , water solution of $\text{CH}_2(\text{COO})_2\text{Tl}_2 + \text{HCOOTl}$ (Belov *et al.* 1975); +, min oil (Haberman & Morton 1954); \square , glycerol (Kutateladze & Nakoryakov 1984).

liquids are investigated. It seems important to compare our results with these experimental observations.

As has been mentioned above, the problem under consideration is governed by two dimensionless parameters: the Reynolds and Weber numbers. The third parameter, the Froude number, appears to be a function of the other two. This feature of the problem is invariant with respect to the dimensionless parameters employed. So one can think that the two independent governing parameters are the Morton number \mathcal{M} , defined by (6.2), and the Eötvös number

$$\mathcal{E} = \frac{g\rho(2a)^2}{\sigma} = \frac{We}{Fr}. \tag{6.4}$$

Conversely, Fr is a function of \mathcal{M} and \mathcal{E} . Prescribing the physical properties of the liquid, namely ν and σ , as well as the gravitational acceleration g , one has the Morton number completely defined, and the Eötvös number is proportional to the equivalent

diameter $2a$. In addition, Fr is proportional to the rise velocity U_∞ . In other words, after the liquid is selected, one can obtain the rise velocity as a function of the equivalent diameter, or, correspondingly, of the equivalent radius a .

Comparison with experiments for the rise velocity requires, however, an iterative procedure, since the original set of parameters for our algorithm are Re and We . This means that for a given Reynolds number we fudge the Weber number in a way to get the appropriate value of Froude number that is needed to get the required Morton number in accordance with (6.2). It is quite an expensive procedure, and we decided to run it only with a couple of specific liquids for the sake of comparison with experiments. Figure 14 shows this comparison for three different liquids. Agreement between the theoretical predictions and experimental results is very good except for the high-Morton-number liquid (denoted by circles).

7. Conclusions

In the present paper a method for solving the Navier–Stokes equations in domains with free or moving boundaries is proposed. A coordinate transformation is introduced so that the region under consideration is mapped into a region with known boundaries which are coordinate surfaces. The latter appears to be crucial for the successful numerical treatment, although the equations of motion become somewhat more complicated, showing oblique derivatives.

An economical difference scheme of splitting type is constructed, and an appropriate algorithm is compounded in order to solve the intricate boundary-value problem. The scheme and algorithm are tested on simple flows that are limiting cases of the motion of a bubble in a viscous liquid. The performance of the method is also checked by means of the usual numerical tests with different meshes, different time increments with respect to the fictitious time, etc.

The method is applied to steady viscous incompressible flow past a resting deformable bubble. This flow is an appropriate model for the flow around stationary rising bubbles in quiescent viscous liquid. The final examination of the method is performed through comparison with known theoretical and experimental results for the same flow in the common range of the governing parameters, the Reynolds and Weber numbers.

On the basis of the method, results are obtained in wide ranges of Reynolds and Weber numbers starting from Stokes flow past undeformable bubbles and finishing up with almost-ideal flow around deformable bubbles. For higher Weber numbers and intermediate Reynolds numbers, a separation of the flow is observed in the rear of the bubble, where a toroidal vortex occurs. The calculated patterns of the separated flow are in good quantitative or qualitative agreement with experimental data or other theoretical predictions. The main geometric characteristics, e.g. aspect ratio and angle of separation, are presented graphically as functions of Reynolds and Weber numbers. The rise velocity of air bubbles is calculated for three different liquids as a function of the diameter of the equivalent bubble and compared with experimental results.

In conclusion, it can be said that the proposed numerical method appears to be a capable tool for handling viscous flows with moving and free boundaries, and can be employed in a variety of similar problems.

The authors are indebted to Dr B. G. Kouznetzov and Dr S. Slavchev for fruitful discussions, as well as to the referees of the paper for most helpful comments.

Appendix. Deriving a condition at infinity of Oseen type

At sufficiently large distances from the bubble, the flow velocity differs slightly from the uniform profile U_∞ . In this instance one can linearize the Navier–Stokes equations regardless of the magnitude of the Reynolds number:

$$U_\infty \left(\cos \theta \frac{\partial}{\partial r} + \frac{\sin \theta}{r} \frac{\partial}{\partial \theta} \right) \zeta = \nu D^2 \zeta. \quad (\text{A } 1)$$

It is well known that the appropriate solution with the required symmetry is given by

$$\psi_2 = -2C_2(1 + \cos \theta) \left\{ 1 - \exp \left[-\frac{rU_\infty}{\nu} (1 - \cos \theta) \right] \right\} \quad (\text{A } 2)$$

(see Van Dyke 1964). This solution gives a flow far from an arbitrary three-dimensional body with no lifting force. In our case it applies because the lifting force is absent owing to the symmetry of the flow. The constant C_2 depends only on certain details of the flow in the vicinity of the body, namely on the value of the drag force. The latter is supposed to be equal to the buoyant force

$$F_a = (\rho - \rho_0) g V, \quad (\text{A } 3)$$

where ρ_0 is the gas density, which will be neglected in what follows since it is much smaller than the fluid density ρ . V is the volume of the bubble.

Let us now assume that a sphere of radius b is situated at the origin of the coordinate system, and b is selected so that the drag force exerted from the liquid on the bubble is equal to the drag force exerted on this imaginary rigid sphere. Then

$$F_a = 6\pi\mu b U_\infty, \quad \text{i.e.} \quad b = \frac{gV}{6\pi\nu U_\infty}. \quad (\text{A } 4)$$

It remains only to match the constant C_2 with this solution. For small r the stream function from (A 2) is represented as

$$\psi_2 \approx -2C_2(1 + \cos \theta) \frac{rU_\infty}{2\nu} (1 - \cos \theta) = -C_2 \frac{rU_\infty}{\nu} \sin^2 \theta.$$

This formula has to be matched to Stokes' solution for a sphere of radius b ,

$$-\frac{3}{4}rbU_\infty \sin^2 \theta,$$

which immediately gives

$$C_2 = \frac{3}{4}\nu b,$$

and then

$$\psi = \frac{1}{2}U_\infty r^2 \sin^2 \theta - \frac{3}{2}\nu b(1 + \cos \theta) \left\{ 1 - \exp \left[-\frac{rU_\infty}{\nu} (1 - \cos \theta) \right] \right\}. \quad (\text{A } 5)$$

Recalling (A 4), we get

$$\psi \sim \frac{1}{2}U_\infty r^2 \sin^2 \theta - \frac{gV}{4\pi U_\infty} (1 + \cos \theta) \left\{ 1 - \exp \left[-\frac{rU_\infty}{\nu} (1 - \cos \theta) \right] \right\}. \quad (\text{A } 6)$$

Introducing the last equality into (2.3), we have

$$\zeta \sim -\frac{gV}{4\pi U_\infty} \frac{U_\infty^2}{\nu^2} \frac{\sin \theta}{r} \left(1 + \frac{1}{Re r} \right) \exp \left[-\frac{rU_\infty}{\nu} (1 - \cos \theta) \right]. \quad (\text{A } 7)$$

Formulae (A 6) and (A 7) give the boundary condition of Oseen type.

REFERENCES

- BELOV, I. V., ELOVIKOV, G. N. & OKULOV, B. E. 1975 In *Teplo- i Masso-Obmennie Protzessi v Vannakh Staleplavitel'nykh Agregatov*, pp. 85–92. Moscow: Metallurgia.
- BHAGA, D. & WEBER, M. E. 1981 *J. Fluid Mech.* **105**, 61–85.
- BRABSTON, D. C. & KELLER, H. B. 1975 *J. Fluid Mech.* **69**, 179–189.
- EL SAWI, M. 1974 *J. Fluid Mech.* **62**, 163–183.
- GORODETZKAYA, A. V. 1949 *Zh. Fiz. Khim.* **23**, pt 1.
- HABERMAN, W. L. & MORTON, R. K. 1954 *Proc. ASCE* **80**, 1–25.
- HADAMARD, J. 1911 *C. R. Acad. Sci. Paris* **152**, 1735–1738.
- HAPPEL, J. & BRENNER, H. 1965 *Low Reynolds Number Hydrodynamics*. Prentice-Hall.
- JEZDINSKY, V. & RUDIS, M. 1973 *Vodnohospodarsky Casopis* **21**, 159–172.
- KUTATELADZE, S. S. & NAKORYAKOV, V. E. 1984 *Teplomassoobmen i Volny v Gazozhidkostnykh Sistemakh*. Novosibirsk.
- LEVICH, V. G. 1959 *Fiziko-Khimicheskaya Gidrodinamica*. Moscow: Gostekhnizdat.
- MIKSIS, M. J., VANDEN-BROECK, J.-M. & KELLER, J. B. 1982 *J. Fluid Mech.* **123**, 31–41.
- MOORE, D. W. 1965 *J. Fluid Mech.* **23**, 749–766.
- PUKHNATCHOV, V. V. 1974 *Zadatchi so svobodnoy granitsei dlya uravneniya Nav'e–Stoksa*. D.Sc. dissertation, Novosibirsk.
- RYBCZYNSKI, W. 1911 *Bull. Acad. Crakowie*, ser. A, pp. 40–44.
- TAYLOR, T. D. & ACRIVOS, A. 1964 *J. Fluid Mech.* **18**, 466–477.
- VAN DYKE, M. 1964 *Perturbation Methods in Fluid Dynamics*. Academic.
- VOLKOV, P. K. & CHRISTOV, C. I. 1980 In *Tchislennie Metodi v Mekhaniki Zhidkosti i Gaza*, Novosibirsk, pp. 19–26.
- VOLKOV, P. K., KOUZNETZOV, B. G. & CHRISTOV, C. I. 1980 *Tchisl. Met. Mekh. Splosh. Sredy* **11**, 22–33.
- YANENKO, N. N. 1971 *Method of Fractional Steps*. McGraw-Hill.